International Journal of Engineering Research and Technology. ISSN 0974-3154 Volume 10, Number 1 (2017)

Electrochemical impedance analysis of SILAR deposited Cu_2SnS_3 (CTS) thin film

H. D. Shelke
Research scholar, Thin Film Physics Laboratory, Department of Physics, Shivaji University, Kolhapur-416 004 (M.S.), India.

A. M. Patil
Research scholar, Thin Film Physics Laboratory, Department of Physics, Shivaji University, Kolhapur-416 004 (M.S.), India.

A. C. Lokhande
Research scholar, Optoelectronic Convergence Research Centre, Department of Materials Science and Engineering, Chonnam National University, Gwangju 500-757, South Korea

J. H. Kim
Professor, Optoelectronic Convergence Research Centre, Department of Materials Science and Engineering, Chonnam National University, Gwangju 500-757, South Korea

C. D. Lokhande*
Professor, Centre for Interdisciplinary Research, D. Y. Patil University, Kolhapur-416 006 (M.S.), India.

Abstract
SILAR deposited copper tin sulfide (Cu_2SnS_3) thin films were used to analyze the study of electrochemical impedance, capacitance- voltage characteristics and current- voltage characteristics. The photoconversion efficiency of SILAR deposited CTS thin film-based photoelectrochemical cell elucidate with the help of capacitance-Voltage (C-V) Characteristics study by Mott- Schottky plot and corresponding circuit model of the impedance spectra of the photoelectrochemical cell.

Keywords:
Electrochemical impedance, photoelectrochemical cell, SILAR, thin film.

Introduction

In recent years, many researchers have used electrochemical impedance spectroscopy (EIS) to explain the working of electrode, to examine the solar cells for a photoelectric research of charge transferring metal-doped fullerenes, for the study of water splitting **[1]**, and for the analysis of water oxidation by photoelectrochemical investigations **[2].** The interest in (photo) electrochemical analysis has increased due to the availability of sophisticated instrumentation, such as electrochemical impedance spectroscopy (EIS) **[3, 4]**.

Although this, there are few reports on the electrochemical analysis of chalcogenide semiconductors. There is a great deal of interest in research of chalcogenide semiconductors due to their appropriate band gaps and high optical absorption coefficients for potential application in thin film solar cells. Chalcogenide based semiconductors such as CdTe and $Cu(In,Ga)Se_2$ are alternatives to Silicon in thin film solar cells **[4, 6]**. CdTe have toxic Cd **[7, 8]**, and $Cu(In,Ga)Se_2$ have costly In and Ga **[9]**, so much awareness has been given to more abundant and lower toxicity materials for thin film solar cells. The copper based multinary compound semiconductor materials are used as absorber materials in photovoltaic technology. Cu_2ZnSnS_4 (CZTS) has been regard as as the alternative absorber layer to $Cu(In,Ga)Se_2$ due to its earth abundant and eco-friendly ingredients, optimal direct band gap of 1.45eV and high absorption coefficient in the visible range **[10, 11]**. But, compositional control and growth of single phase CZTS films are quite difficult process. The control of composition and phase structure in Cu_2SnS_3 compound is more convenient due to its fewer elements compared with CZTS. Ternary semiconductors such as Cu-Sn-S (CTS) belonging to I-IV-VI groups are preferred as excellent absorber material due to high absorption coefficient ($>10^4$ cm^{-1}) and small band gap (0.9 to 1.5 eV) for photovoltaic cells, and as a suitable candidate for nonlinear optical materials **[12].** It is a p-type semiconductor with band gap and optical absorption coefficient similar to that of CZTS material which is currently being comprehensively studied in the photoelectronic field. The Cu_2SnS_3 has been synthesized by various chemical methods such as chemical bath deposition (CBD) **[13]**, spin coating

[14], hydrothermal **[15]**, electrodeposition **[16]**, successive ionic layer adsorption and reaction (SILAR) **[17]**, spray pyrolysis **[18]**, hot injection **[19]**, solvothermal **[20]** etc.

Compared to other chemicals methods, SILAR is a simple, less expensive and less time consuming method for the deposition of semiconducting thin films. It is also significant in the deposition of large area thin films. In SILAR method, substrate is sequentially dipped into the precursor solution during the deposition process. Sufficient reaction time favors the complete chemical reaction and hence produces pure phase compounds without secondary phases. In this method, deposition cycles and dipping time are key parameters for synthesis of nanoparticles to covering films.

Based on previous work we identify that CTS photoanode is excellent absorber material and suitable candidate for nonlinear optical materials. Thus, in present paper, we report the results of an EIS study, which carried out to examine the carrier transport properties, to determine the equivalent circuit parameters and to analyze the performance of the PEC cell. The current-voltage (I-V) characteristics of PEC cell used to find out cell efficiency. Mott-Schottky plot was used to determine flat band potential and charge carrier density of CTS photoelectrode.

Experimental details

The chemical approach apply to synthesize CTS thin films the mixed solution of copper sulphate ($CuSO_4.2H_2O$), tin chloride ($SnCl_2.2H_2O$) and Triethanolamine (TEA) is utilize as the cationic precursor and sodium sulphide ($Na_2S.xH_2O$) solution is utilize as an anionic precursor. CTS film is deposited on conducting oxide i.e. indium doped tin oxide (ITO) substrate. The substrate is ultrasonically cleaned in double distilled water (DDW) for 15 minutes and then washed by acetone. In deposition process of Cu_2SnS_3, TEA solution is used as a complexing agent who binds metal cation in the solution. The molar concentrations of $CuSO_4.2H_2O$, $SnCl_2.2H_2O$ and $Na_2S.xH_2O$ in the solution are 0.2, 0.1 and 0.3 M, respectively. In the SILAR method, the substrate is immersed into separate cationic and anionic precursor solutions for the adsorption and reaction, and then rinsed with DDW after each immersion to remove the loosely bound particles and to avoid the precipitation. By repeating the cycle described above, CTS thin film with the desired thickness is obtained by adjusting the preparative parameters. These films are annealed at 300 °C in a vacuum to improve the crystallinity. The CTS films are well adherent, uniform and blackish in color.

Materials characterization

To investigate the characteristic parameters of the CTS thin films by XRD (X-ray diffraction), EDAX (Energy dispersive X-ray spectroscopy), XPS (X-ray photoelectron spectroscopy), FE-SEM (field effect scanning electron microscopy), optical absorption, Mott-Schottky, Electrochemical Impedance spectroscopy (EIS), and current-voltage plot of PEC cell characterization techniques is used. The XRD patterns is recorded by a BRUKER AXS D8 Advanced model X-ray diffractometer equipped with Cu radiation (K_α of λ= 1.54 Å). The XPS analysis is studied by using VG Multilab 2000, Thermo VG Scientific, UK, for state confirmation of CTS material. The morphology of the samples is analyzed by FE-SEM (JEOL JSM-6390). Optical band gap is determined by the UV-Visible absorption spectroscopy analysis carried out by a (UV- 1800 Shimadzu) spectrometer. I-V characteristics of the PEC cell were examined using a Princeton Applied Research Potentiostat (273A) with a CTS electrode as the working electrode. Mott- Schottky plot and EIS study in dark and under illumination conditions was carried out with an electrochemical workstation model Zive-5. Zman software was used to model the equivalent circuit from EIS.

Results and discussion

Structural study

Fig. 1 confirms phase formation of Cu_2SnS_3 material by X-ray diffraction (XRD) pattern. After annealing the films at 300^0C in vacuum, all of the diffraction peaks were in good match with the standard pattern of triclinic CTS (JCPDS No.: 27-0198) observed in **Fig. 1**. This annealing process increased the peak intensities and sharpness. XRD pattern shows remarkable texture growth along (-2 0 10) plane at $2\theta = 47.18^0$, as evidenced by JCPDS data file card [027–0198]. In addition to few other peaks at (-2 -1 1), (-2 0 6), (-3 -2 10) and (-4 0 12) planes at $2\theta = 28.36^0$, 32.82^0, 55.97^0 and 69.01^0 respectively. The XRD pattern shows good matching between observed and standard interplanar spacing (d) values with triclinic crystal structure. Inter planar distances (d) of the planes, were calculated using Bragg's diffraction condition **[21].** Calculated d values are shown in **Table 1**, which is comparable with standard JCPDS data. Crystalline grain sizes (D) of the films were evaluated using Debye–Scherrer formula **[22]**

$$D=\frac{0.9\lambda}{\beta Cos\theta} \qquad (1)$$

Where K is the shape factor taken equal to 0.9, λ is the wavelength of the X-ray used, β is the full width at half maximum of the peak and θ is the Bragg angle that corresponds to the peak analyzed. The differences between the relative X-ray diffraction

intensities of the samples and standard JCPDS data show a preferential orientation, which can be evaluated considering the texture coefficient (T_c). The texture coefficients of the CTS thin films were calculated using the equation

$$T_c(hkl) = \frac{I(hkl)/I0(hkl)}{\frac{1}{N}\Sigma I(hkl)/I0(hkl)} \qquad (2)$$

Where, I is measured intensity, I_0 is JCPDS standard intensity, N is the reflection number. For randomly orientated materials, T_c values of all the planes are approximately 1.While the larger values of T_c show preferential orientation, smaller values show lack of grains orientated in that direction **[23].** Calculated T_c values of CTS thin films are shown in **Table 1**. No one secondary phase is observed within CTS formation by using SILAR method.

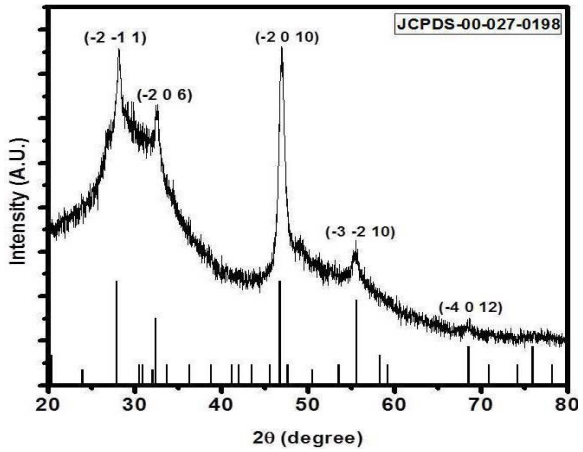

Fig. 1 XRD pattern of CTS thin film.

Table 1 Standard and calculated interplanar distances with texture coefficient values of CTS thin film calculated from XRD Plot.

Sample	2θ	FWHM β	D-spacing Å	Standard D-spacing Å	Crystallite size D	Texture coefficient T_c
CTS	28.17	0.31	3.16	3.14	4.53	4.89
	32.55	0.47	2.75	2.75	3.05	13.78
	46.81	0.47	1.94	1.96	3.19	5.00
	55.58	0.70	1.65	1.63	2.21	1.38

X-ray photoelectron spectroscopy (XPS)

The XPS is surface receptive quantitative spectroscopic system that measures the elemental composition, electronic state, chemical state and empirical formula of the elements that available within the material. The XPS survey spectrum of CTS thin film is shown in **Fig. 2 (A)**. From XPS spectroscopy, it is obvious that CTS material consists of the Cu^{1+}, Sn^{4+} and S^{2-} elements with the quantification of Cu2p, Sn3d and S2p core levels peaks, respectively **[24]**. The Cu2p, Sn3d and S2p core-level photoelectron spectra with the appropriate profile for quantitative elemental composition determination are shown in **Fig. 2 (B)**, **(C)** and **(D)**, respectively. The binding energy of Cu $2p_{3/2}$ and Cu $2p_{1/2}$ peaks are 932.77 and 952.50 eV, respectively **[25]**. The satellite peaks does not observed around 932 and 955 eV at Cu2p core level, which correspond to the existence of copper is Cu^{1+} state in CTS material **[26]**. The binding energies for Sn $3d_{5/2}$, Sn $3d_{3/2}$ and S $2p_{3/2}$ are 487.15, 495.61 and 163.36 eV, respectively, which match well with the earlier reports **[27]**. The XPS studies authenticate that presence of Cu and Sn in +1 and +4 oxidation states, respectively.

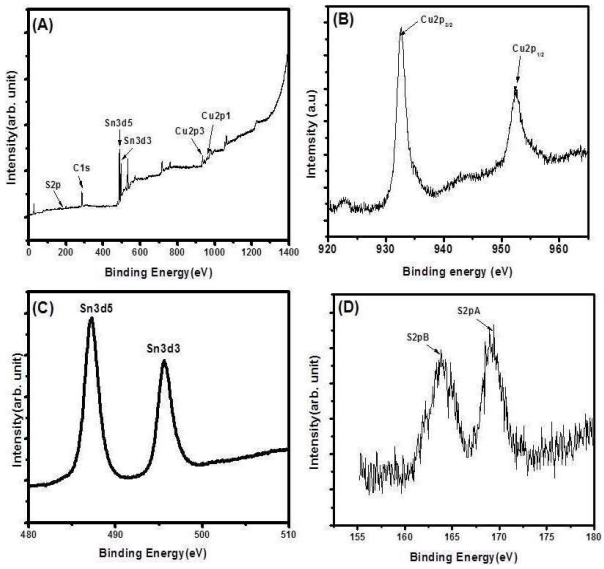

Fig. 2 X-ray photoelectron spectra of CTS material. **(A)** Survey spectrum, **(B)** Cu 2p core level, **(C)** Sn 3d core level and **(D)** S 2p core level.

FE-SEM Analysis:

Fig. 3 (A) & (B) shows FE-SEM images of CTS films at 15,000 and 20,000X magnifications. **Fig. 3(A)** shows a uniform distribution of agglomerated nanocrystals i.e. it shows the complete crystal growth over the entire surface of substrate. It shows evidence of appreciable grain formation. The grain formation is seen in **Fig. 3(B)**.The uniform density, adhesion to the substrate and compact nature of the film is observed. It is observed that the film is homogeneous and have dense microstructures. The film surface looks smooth and uniform. It is well clear from the micrographs that the particles are spherical and adherent. It can be seen that these spherical grains are uniformly distributed to cover the surface of the

substrate completely. In **Fig. 3(B)** indicate that CTS film is composed of a dense packing of grains with small voids, signifying uniformity of thin film surface. A close assessment of the figures showing that, the nature of the grains of deposited material has a less porous nature with clusters, which consist of extremely small spherical grains, annealing at 300 ^{0}C for an hour in vacuum, changed the nature of the grains considerably. Also, a small crystallites growth on compact surface is observed. Salgam et al **[28].** It is also seen that the number of bulky small grains overlapped and combined together to form relatively immense islands of CTS material. This type of surface arrangement is due to the particularly small dimensions and elevated surface energy.

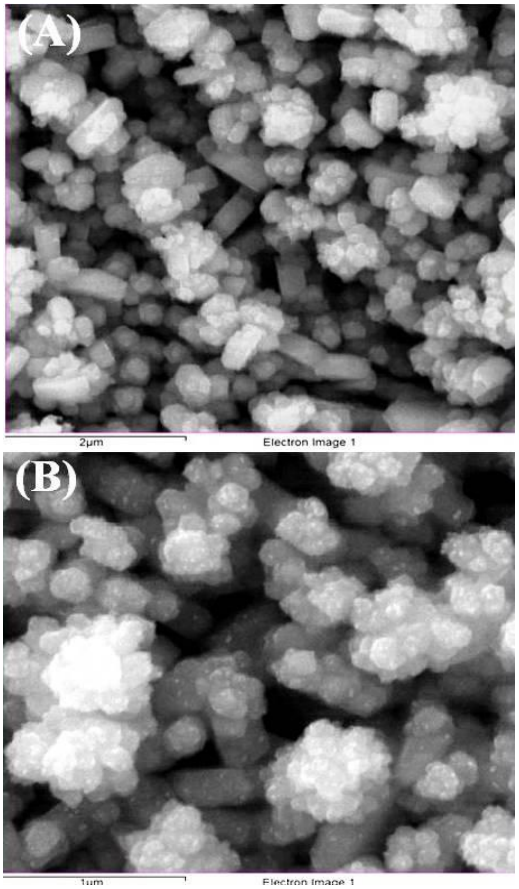

Fig. 3 FESEM images of CTS-thin film at two magnifications of **(A)** 15,000X and **(B)** 20,000X.

Optical properties: UV–visible spectra

The optical absorption spectra of SILAR deposited CTS thin film has been carry out at room temperature from 300 to 900 nm wavelength is shown in **Fig. 4**. The nature of optical shift and the value of the optical band gap of the material can be determined using optical absorption measurements. The CTS thin films show wide absorption range and the covers almost whole visible region is shown in inset of **Fig.4**. These spectra revealed that the deposited CTS thin films have high absorbance of light in the visible region, indicating its applicability as an absorbing material in industries such as solar cell windows layer. The CTS thin film has high absorption in the visible region with a hump at 500 nm, which is close to the effective band gaps of CTS thin film, making it a good light absorbing material. The optical band gap spectrum was plotted from the absorption spectrum. The observed results of the film gives the indication of samples shows nearly sharp absorption variation around 500 nm. The optical band gap is evaluated using the Tauc relation **[29]**.

$$h\upsilon = A(h\upsilon - E_g)^n \qquad (3)$$

Where, A is a constant which is associated to the effective masses allied with the valence and conduction bands and, n depends on the nature of transition which is identical to 1/2 for direct transition and 2 for indirect transition. **Fig. 4** shows the linear variation of $(\alpha h\upsilon)^2$ versus $(h\upsilon)$, which indicates that the material has a direct optical band gap **[30].** It is clear from the figures that optical absorption coefficients of the films are high (~10^4 cm^{-1}). The band gaps of the CTS thin films were found to be 1.56 eV. The band gap showed a good match with the optimal band gap for a solar cell, indicating CTS to be a capable material for thin film solar cell applications.

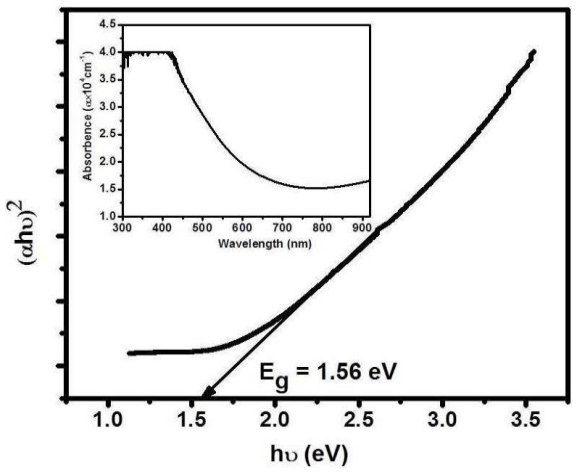

Fig. 4 Band gap plot of CTS thin film. The inset in Fig. 4 shows optical absorption spectra.

I-V Characteristics of PEC Cells

The photoelectrochemical (PEC) responses of CTS thin film in wide potential range of 0.6 to -0.6 V under dark and light (chopped illumination) are observed in **Fig. 5**. The photovoltaic output

characteristics of CTS thin films are studied by fabricating **ITO/CTS/LiClO$_4$/graphite** Cell. The solid-liquid junction for the PEC cell was formed with the CTS electrode as the photoelectrode and 0.25 M LiClO$_4$ (Lithium per chlorate) solution as the electrolyte. A graphite bar was employ as the counter electrode in the cell. The current-voltage curve in a dark state specifies a usual electrochromic response of the CTS film due to the intercalation/ deintercalation of electrons. The current-voltage curve in light (chopped illumination) exhibit that the PEC response in progress to come insight the potential range above -0.1 V is observed in **Fig. 5** (B). It is well-known that the electrochromic reaction mainly occurs at the interfaces between the working electrode and the electrolyte. This in turn indicates that the amount of the electrochemical reaction sites of the CTS electrode may be evaluated by comparing current densities of the electrochromic reaction. The PEC cell with the configuration, CTS| 0.2 M LiClO$_4$| graphite, was illuminated with a light of intensity 50 mW/cm^2. The electrochromic current density versus voltage curves CTS thin films is observed in **Fig. 5** (A). The current density is increased under illumination, which leading to extremely improved electrochemical reaction sites for the CTS electrode. The CTS semiconductor absorbs the photons with energy equal to or greater than the band gap energy of CTS. This causes the creation of electron-hole pairs in the depletion region and in the diffusion layer ($e^- + h^+$). They are constraining apart by the electric field at the edge. Electrons are drifted towards semiconductor surface, while holes are drifted towards bulk semiconductor from depletion region. The photocurrent can be effectively increased due to the development of a depletion layer and decreased recombination centers **[31]**. Improved electrochemical reaction sites are observed due to the superior crystallinity of the film with better crystallite size, as shown in **Fig. 5**. The PEC cell parameters, such as short circuit current (Isc), open circuit voltage (Voc), maximum current (Im), maximum voltage (Vm), were estimated for the active surface area of 1cm^2 and light intensity of 50 mW/cm^2 for CTS thin films is shown in inset of **Fig**. 5(A) The highest values of photo conversion efficiency 0.11% with fill factor of 30 % are achieved by CTS thin film. As argue in XRD and FE-SEM, a good crystalinity and homogeneous, compact morphology reduces the constraints of the grain boundary to construct an easier pathway for the flow of current and by elevate the electron diffusion length for superior photochemistry.

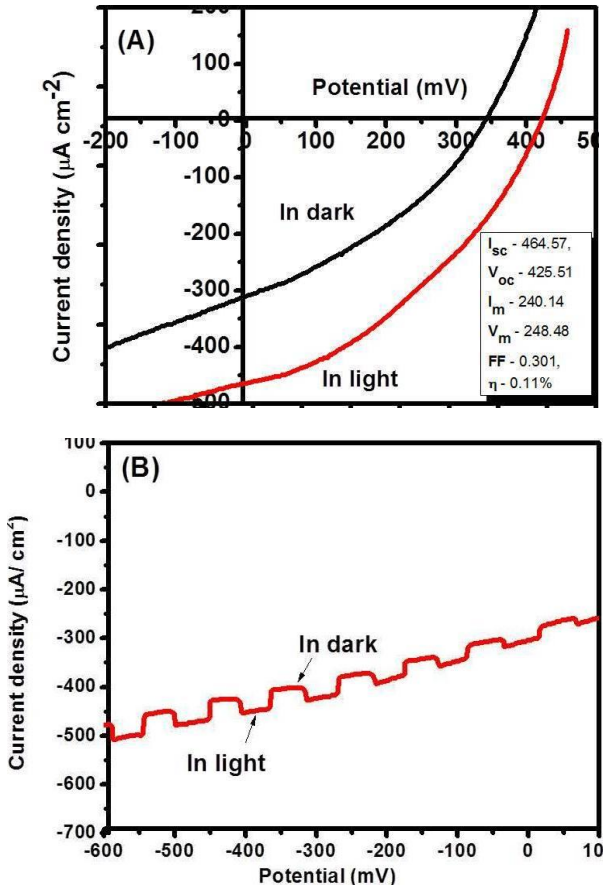

Fig. 5 (A) Current- voltage characteristics of the CTS thin film and **(B)** shows the CTS thin films under chopped illumination.

Electrochemical Impedance Spectroscopy (EIS) Study of PEC Cell

Electrochemical impedance spectroscopy (EIS) has been calculated by applying an AC potential to an electrochemical cell and then calculate the current throughout the cell. The impedance has information related to the phase difference, which refers to the angle by which the current leads the voltage **[32]**. The impedance is a vector, describe by the phase angle α, which can be resolved into two components. The impedance factor in phase with the cell voltage is describing the real part (Z_{real}) and the impedance factor at 90° to the cell voltage is describing the imaginary part ($Z_{imag.}$). Determination of impedance Z as a function of the frequency and then resolve it into Z_{real} and Z_{imag} is the method of studying the impedance of an electrochemical circuit. These magnitudes were plotted by using two techniques i.e. Bode plot and Nyquist Plot **[33].** A plot of Z_{real} Vs. Z_{imag} for the equivalent frequency is known as the Nyquist plot. Each point on the resulting diagram is made up of a Z resolved in two components

measured at a selected frequency. Each point on the Nyquist plot corresponds to impedance at one frequency. There may be such 20 - 30 points each at different frequencies.

Nyquist plots

EIS is an analytical instrument for study the photovoltaic performance of PEC cell and investigate the changes that occur during illumination with 50 mW/cm^2. Frequency dependent electrochemical measurements of CTS thin film electrode under dark and illumination have been carried out at room temperature. EIS is measured in the two-electrode method recording impedance plots include the response of the counter electrode as well as the photoanode. Generally, impedance data were differentiating in the complex-plane impedance called Nyquist diagram. The Nyquist plots for under dark and illumination of CTS thin film is revealed in **Fig. 6(A)**. Inset **Fig. 6(A)** shows the equivalent circuit and **Table 2** summarizes the equivalent circuit parameters gained by best fitting the impedance data. The equivalent circuit elements consist of Rs, R1, Q1, R2 and Q2. The high frequency (corresponding to low Z') intercept on the real axis (i.e., Z'axis) signifying the series resistance (Rs). Rs are the ohmic series resistance of the electrode system which provide to the electrical contact of the electrode-electrolyte and resistivity of electrolyte solution. R1 represents the charge transfer resistance and Q1 is the double layer capacitance at the electrode-electrolyte interface. R2 and Q2 represents recombination charge transfer resistance and chemical capacitance at the electrode-electrolyte interface.

The half circle in high frequency range is resulted from the charge transfer resistance (Rct) and the equivalent constant phase angle element (CPE) at the electrolyte-electrode edge. Rs values for CTS thin film electrodes are in the range of ohms and decrease it after illuminate the film. It is seen from **Table 2** that as, under illumination, Rs decreases of from 3.72 to 1.09 Ω. The large Rs of CTS thin film under dark condition can be attributed to the presence of natural ligand on the CTS surface. The R_s element is related with a high frequency response, which illustrate minor variation after illumination, signifying that it is independent of illumination. After illumination the CTS electrode, film exhibited the smallest Rct and CPE, signifying a superior catalytic movement and bulky surface areas. The smallest charge transfer resistance (Rct) of 37.83 Ω is observed for CTS thin electrode indicating fast electron diffusion process under illumination. Lower Rct of the CTS electrode expected relatively high electrical conductivity suggesting more quick charge transfer reaction for Li^+ addition/extraction happens at the interface **[34].**

From **Fig. 6 (A)**, CTS films have a single semicircle indicating the single relaxation process (relaxation time). The Rct value of CTS electrode under illumination condition in aqueous electrolyte shows lower as compared to the Rct of CTS film under dark condition, because of Li^+ ions in the 0.25M $LiClO_4$ electrolyte plays an important role for long lifetime of the electron **[35].** The reduction in Q1 after illumination condition of CTS electrode is confirmation for a uniform distribution of current through bulk electrode. While, the raise in Q2 shows the increase in the accumulation of charges at the interfacial region, which may be due to the chemical capacitance of the surface trap states that are available due to the compact nature of the film **[36].** The EIS results agreed well with the photocurrent-voltage experiments. Therefore, it is concluded that for higher photocurrent generation, suitable electrolyte should be selected.

Bode plot

Bode phase plot provide the information of electron life period inside the electrode-electrolyte transition. Bode plot is nothing but phase angle against the logarithmic frequency (log f) is observed in **Fig. 6 (B)**. After illuminating CTS thin electrode, the phase angles shifted to higher values (shown in **Table 2**) due to the crystalinity, average grain size and surface compactness of the electrode. The phase angle of CTS thin film under dark condition is -3.65^0 less than that for the CTS thin electrode under illumination (-2.44^0), shows the superior electrochemical behavior. Bode magnitude plot exhibit that the resistance of CTS electrode films sharply drop off in higher frequency region, indicate distinct change in slope with increase the conductivity **[37].**

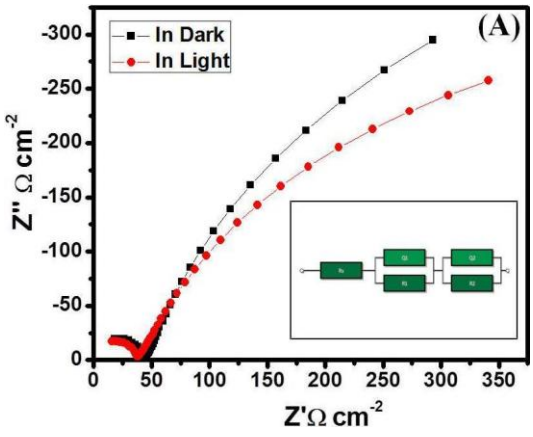

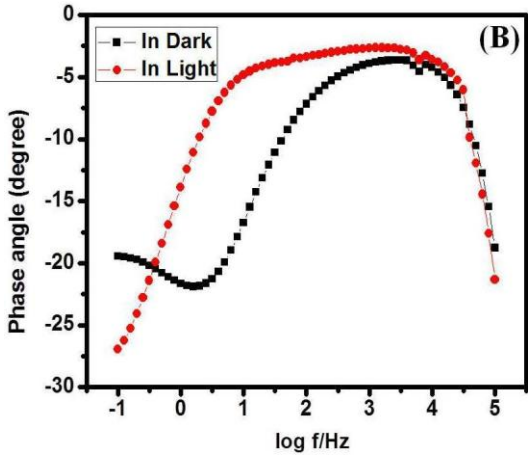

Fig. 6 (A) Nyquist plot for electrochemical impedance study of a PEC cell under dark and illuminated conditions (Inset in Fig. 5 shows the equivalent circuit of the PEC cell) and **(B)** shows the Bode plot of CTS electrode in dark and under illumination.

Table 2 Equivalent circuit parameters for EIS analysis under dark and light conditions.

Sample	Rs (Ω-cm^{-2})	Rct (Ω-cm^{-2})	Q1 (μF-cm^{-2})	R2 (Ω-cm^{-2})	Q2 (μF-cm^{-2})	Phase angle
Under dark	3.72	44.03	50	2.77	25	-3.65
Under light	1.09	37.83	23.3	0.20	223	-2.44

Capacitance-Voltage (C-V) Characteristics Study by Mott- Schottky plot

The calculation of capacitance as a function of applied voltage is observed by using Mott-Schottky plot. The Mott- Schottky plot exposed a non-linear relation, as represent in **Fig. 7**.The capacitance-voltage (C-V) characteristics of the PEC cell were studied in the dark. The ionic adsorption, surface roughness and non-planar interfaces on the surface of working electrode are the probable basis for the non-linear activities of the plot **[38]**. The Mott- Schottky plot provides useful information on the photoelectrode such as the type of conductivity, carrier concentration (N_d) and flat band potential (V_{fb}). The electrode potential V_{fb}, at which the band bending is zero, was 0.62 V and carrier density was 1.18 x 10^{22} per cm^3. The capacitance-voltage (C-V) measurements of CTS film electrode are carried out at the interface of electrode-electrolyte at the fixed frequency of 1 kHz in bias sweep from 0 - 0.8 V/SCE. The Mott-Schottky plots for CTS film electrodes are shown in **Fig. 8**. From the Mott-Schottky plots (1/ C^2 vs. V), the best fitted straight line gives the slope of curves. A slope with negative photocurrent for CTS film proves the p-type electrical conductivity of CTS electrodes **[39].** For PEC cell measurement, flat band potential (Vfb) is significant physical parameter to study the transfer of charge carriers at the boundary of semiconductor electrode and electrolyte. The flat band potentials of CTS semiconductor electrode are estimated from Mott-Schottky plot by extrapolating the curves to the intercept with $1/C^2 = 0$. The value of Vfb observed in positive side is probably due to the electronic structure of the CTS thin film **[40].** The capacitance in the Mott-Schottky plot to the applied voltage is associated to capacitance of space charge layer and capacitance of double layer. The suitable Vfb and donor concentration shows the better ability of the CTS electrode to easier transfer of charge carrier at the interface of electrode to electrolyte **[41]**. From **Fig. 7**, 'graded type' junction is observed due to the nonlinear nature of Mott Schottky plot which attributed to the occurrence of "shallow" as well as "deep" donor stages (density of interface state) **[42].**

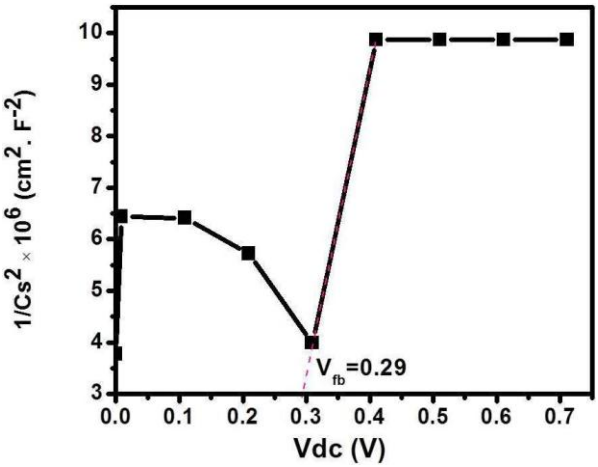

Fig. 7 Mott-Schottky plot for the capacitance-voltage characteristics study of PEC cell.

Conclusion

CTS thin film has been successfully deposited on ITO conducting substrate by SILAR method. The electrochemical impedance properties of CTS thin films are studied by using EIS technique. X-ray diffraction patterns confirm the formation of nanocrystalline structure with triclinic CTS phase. The XPS confirms presence of Cu and Sn in +1 and +4 oxidation states, respectively. Field emission scanning electron microscopy analysis reveals that CTS thin film has uniform morphology with spherical grains. The photoelectrochemical measurement exhibits that CTS film electrode shows a power conversion efficiency of 0.11% with large photocurrent. Electrochemical analysis reveals that the CTS films under illumination shows lower charge

transfer resistance which effectively reduces the relaxation time and take action to fast electrochemical route. Mott-Schottky plot make known that the suitable Vfb and donor concentration shows the better ability of the CTS electrode to easier transfer of charge carrier at the electrode-electrolyte interface.

Acknowledgement
Present work was supported by the Human Resources Development program (No.20124010203180) of Korea Institute of Energy Technology Evaluation and Planning (KETEP) Grant funded by the Korea government Ministry. The basic Science Research Program through the National Research Foundation of Korea (NRF) funded by the Ministry of Science, ICT (NRF2015R1A2A2A01006856).

Reference

1. T. Lopes, L. Andrade, H. Riberio, A. Mendes, Int. J. Hydrogen Energy 35 (2010) 11601.
2. B. Klahr, S. Gimenez, F. Santiago, J. Bisquert, T. Hamann, Energy and Environmental Science, 5 (2012) 7626.
3. L. G. Chatten, J. Pharm. Biomed. Anal. 1(4) (1983) 491.
4. R. Memming, Top. Curr. Chem. 143 (1988) 79.
5. B. Shin, O. Gunawan, Y. Zhu, N. Bojarczuk, S. Chey, S. Guha, Prog. Photovolt Res. Appl., 21(1) (2013) 72.
6. D. Barkhouse, O. Gunawan, T. Gokmen, T. Todorov, D. Mitzi, Prog. Photovolt Res. Appl., 20 (2012) 6.
7. L. Baranowski, K. McLaughlin, P. Zawadzki, S. Lany, A. Norman, H. Hempel, R. Eichberger, T. Unold, E. Toberer and A. Zakutayev, Phys. Rev. Applied, 4 (2015) 044017(1).
8. M. Adelifard, M. Mohagheghi, H. Eshghi, The Royal Swedish Acad. of Sci. Physica_Scripta, 85 (2012) 035603.
9. P. Fernandes, P. Salome, A. D. Cunha, J. Phys. D: Appl. Phys., 43 (2010) 1.
10. K. Wang, O. Gunawan, T. Todorov , B. Shin, S. Chey, N. Bojarczuk, D. Mitzi, S. Guha, Appl. Phys. Lett. 97 (2010) 143508 (3pp).
11. H. Katagiri, K. Jimbo, S. Yamada, T. Kamimura, W. Maw, T. Fukano, T. Ito, T. Motohiro, Appl. Phys. Express 1 (2008) 41201(2pp).
12. Z. Su, K. Sun, Z. Han, F. Liu, Y. Lai, J. Li and Y. Liu, J. Mater. Chem., 229 (2012) 16346.
13. B. Taher, M. Alias, I. Naji, H. Alawadi, A. Douri, Aust. J. Basic appl. Sci., 9 (2015) 406.
14. J. Han, Y. Zhou, Y. Tian, Z. Huang, X. Wang, J. Zhong, Z. Xia, B. Yong, H. Song and J. Tang, Front Optoelectron, 7 (2014) 37.
15. M. Shawky, A. Shenouda, El. Said, I. Ibrahim, Int. J. Sci. Engg. Res., 6 (2015) 1447.
16. D. Berg, R. Djemour, L. Gutay, G. Zoppi, S. Siebentritt, P. Dale, Thin Solid Films, 520 (2012) 6291.
17. Z. Su, K. Sun, Z. Han, F. Liu, Y. Lai, J. Li, Y. Liu, J. Mater. Chem., 22 (2012) 16346.
18. G. Ilari, C. Fella, C. Ziegler, A. Uhl, Y. Romanyuk, A. Tiwari, Sol. Energy Mater. Sol. Cells, 104 (2012) 125.
19. A. Lokhande, K. Gurav, E. Jo, M. He, C. Lokhande, J. Kim, Opt. Mater. 54 (2016) 207.
20. F. Chen, J. Zai, M. Xu, X. Qian, J. Mater. Chem., A1 (2013) 4316.
21. H. Yoo, J. Kim, Sol. Energy Mater. Sol. Cells 95 (2011) 239.
22. C. Wang, S. Shei, S. Chang and S. Chang, Applied Surface Science, 388 (2016) 71.
23. S. Sohila, M. Rajalakshmi, C. Ghosh, A. Arora and C. Muthamizhchelvan, J. Alloys. Compd., 509 (2011) 5843
24. B. Strohmeier, D. Levden, R. Field, D. Hercules, J. Catal., 94 (1985) 2806.
25. R. Scheer and H. Lewerenz, J. Vac. Sci. Technol. A, 12 (1994) 56.
26. D. Tiwari, T. Chaudhuri, T. Shripathi, U. Deshpande, V. Sathe, Appl. Phys. A, 117 (2014) 1139.
27. P. Grutsch, M. Zeller, T. Fehlner, Inorg. Chem., 12 (1976) 1431.
28. M. Saglam, A. Ateş, B. Guzeldir and O. Ozakın, Phys. Status Solidi (A), 209 (2012) 687.
29. M. Ashokkumar and S. Muthukumaran, J. Mater. Sci. Mater. Electron., 24(2013) 2858.
30. C. Lokhande, S. Pawar, Solid State Commun. 49 (1984) 765.
31. M. Law, L. Greene, J. Jhonson, R. Saykally, P. Yang, Nat. Mater. 4 (2005) 455.
32. A. Bard, L. Faulkner, A John Wiley and Sons, New York (2001) 369.
33. J. Bockris and A. Reddy, Springer, New York (2008) 1127.
34. S. Swami, N. Chaturvedi, A. Kumar, N. Chander, V. Dutta, D.K. Kumar, A. Ivaturi, S. Senthilarasu, H. Upadhyaya,, Phys. Chem. Chem. Phys. 16 (2014) 23993.
35. A. Bhalerao, B. Wagh, R. Bulakhe, P. Deshmukh, J. Shim, C. Lokhande, Journal of Photochemistry and Photobiology-A: Chemistry, 336 (2017) 69.
36. Q. Wang, J. E. Moser, M. Gratzel, J. Phys. Chem. B, 109 (2005) 14945.
37. S. Patil, V. Lokhande, D. Lee and C. Lokhande, Optical Materials, 58 (2016) 418.
38. R. Mane, B. Sankpal, C. Lokhande, Mater. Chem. Phys., 60 (1999) 196.

39. S. Huang, W. Luo, Z. Zou, J. Phys. D. Appl. Phys., 46 (2013) 235108.
40. Y. Hsu, S. Lee, J. Chang, C. Tseng, K. Lee, C. Wang, Int. J. Electrochem. Sci. 8 (2013) 11615.
41. S. Kumari, C. Tripathi, A. Singh, D. Chauhan, R. Shrivastav, S. Dass, V. Satsangi, Curr. Sci. 91 (2006) 25.
42. A. Rajbhoj, S. Gaikwad, J. Deshmukh, V. Bhuse, Arch. Appl. Sci. Res. 4 (2012) 9.